



**NTNU – Trondheim**  
Norwegian University of  
Science and Technology

# Modeling and Analysis of a Batch Gravity Separation of an Oil and Water Emulsion

**Marius Espenes**

Chemical Engineering and Biotechnology

Submission date: June 2014

Supervisor: Brian Arthur Grimes, IKP

Norwegian University of Science and Technology  
Department of Chemical Engineering



## Preface

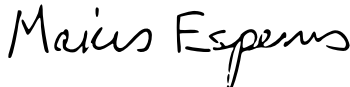
This report was written in cooperation with the Ugelstad Laboratory and Faculty of Natural sciences and Technology Department of Chemical Engineering at Norwegian University of Science and Technology (NTNU). The master thesis was carried out from January to June of 2014 within the the field of Colloidal chemistry. To ensure the project outcome, it was important to have good structure regarding modelling, documentation and good collaboration with my advisor and colleagues from the start.

The author will use this opportunity to gratefully thank the supervisor for help and guidance with this project: Brian A. Grimes.

### Declaration of compliance

I declare that this is an independent work according to the exam regulations of the Norwegian University of Science and Technology (NTNU).

Place and date: Trondheim, June 17, 2014

Signature: 





## Abstract

A model for simulating the separation of an emulsion in a batch gravity settler was tested. This model is based on a population balance which considers a non-uniform droplet distribution, where coalescence occurs simultaneously as the film drains during the time of contact. This model also incorporates the physical properties of the bulk fluids, liquid-liquid interface, the effects of surface properties and the squeezing forces subjected on the droplets.

The population balance predicts the dynamic and spatial evolution of the dropsize distribution across the entire batch separator. The model was used to fit data for local fractions from experimental data in order to compare the model results with actual experimental results.

The prediction of the dynamic and spatial evolution of the drop size distribution allows one to calculate the backflow of the continuous phase and drop growth rate (the first moment of the volume weighted coalescence birth function). These two calculated values allow one to make a semi-quantitative description of the individual sedimentation and binary coalescence rates, based on the types and concentration/composition of demulsifiers or mixtures of demulsifiers used for separation.

The experiment consisted of an water in crude oil emulsion with added demulsifier. Five experiments were tested, with varying ratios of the two different demulsifiers, Demulsifier 1 and Demulsifier 2.

The results for the different demulsifiers demonstrated that pure Demulsifier 2 provided the fastest separation of this water in oil emulsion, this was due to the large initial droplet size in this mix. However, the blend with 50% Demulsifier 1 and 50% Demulsifier 2 had the largest maximum continuous phase velocity ( $U_{f,max}$ ) and maximum drop growth rate ( $R_{g,max}$ ), which resulted in a fast separation, 25min for complete separation as opposed to 16min for the pure chemical Demulsifier 2. The large value of  $U_{f,max}$  indicate fast sedimentation and  $R_{g,max}$  indicate fast binary coalescence, however the large initial droplet size for the pure Demulsifier 2 provided the fastest separation.

This separation model could then be used to develop chemical destabilization strategies to knock out a significant fraction of the emulsified water and reduce process volumes and energy consumption, which could reduce greenhouse gas emissions and improve process economy.



## Sammendrag

En modell for simulering av separasjon av en emulsjon i en "batch gravity settler" ble testet. Denne modellen er basert på en populasjonsbalanse som betrakter en ikke-uniform dråpefordeling, hvor koalesens skjer samtidig som "film-drainage" i løpet av tiden for kontakt. Denne modellen innbefatter også de fysiske egenskaper for bulk væskene, væske-væske-grensesnittet, virkningene av overflateegenskaper og "squeezing"-krefter som er utsatt på dråpene.

Populasjonsbalansen kan forutsi den dynamiske og romlige utviklingen av dråpestørrelsefordelingen over hele batch separatoren. Modellen ble brukt til å plassere data for lokale fraksjoner fra eksperimentell data, for å sammenligne modellresultatene med faktiske eksperimentelle resultater.

Prediksjon av den dynamiske og romlige utviklingen av dråpestørrelse distribusjon gjør det mulig å beregne tilbakestrømmingen av den kontinuerlige fasen samt dråpevekstraten (det første øyeblikk av den volumveide-koalesensfødselsfunksjonen). Disse to beregnede verdier tillater en å få en semi-kvantitativ beskrivelse av den enkelte sedimentering og binære koalesens rater, basert på hvilke typer og konsentrasjoner/sammensetningen av demulgatorer eller blandinger av demulgatorer som benyttes for separasjon.

Eksperimentet besto av en vann i råolje emulsjon med tilsatt demulgator. Fem eksperimenter ble testet, med varierende forhold av de to forskjellige demulgatorer, Demulsifier 1 og Demulsifier 2.

Resultatene for de forskjellige demulgatorer viste at ren Demulsifier 2 ga den raskeste separasjon av denne vann i olje emulsjonen, dette var på grunn av den store initielle dråpestørrelsen i denne blandingen. Imidlertid hadde blandingen med 50 % Demulsifier 1 og 50 % Demulsifier 2 størst maksimal kontinuerlig fasehastighet ( $U_{f,maxs}$ ) og maksimal dråpe vekstrate ( $R_{g,maxs}$ ), som resulterte i en rask separasjon, 25min for fullstendig skille i motsetning til 16min for den med ren kjemisk Demulsifier 2. Den store verdien av  $U_{f,maxs}$  indikerer rask sedimentering og  $R_{g,maxs}$  indikerer rask binær koalesens, imidlertid den store opprinnelige dråpestørrelse for den rene Demulsifier 2 resulterte i den raskest separasjonen.

Denne separasjonsmodellen kan brukes til å utvikle kjemiske destabilisering strategier for å slå ut en betydelig andel av emulgert vann og redusere prosess volum og energiforbruk, noe som kan redusere klimagassutslippene og forbedre prosessøkonomien.



# Table of Contents

<b>Preface</b>	<b>I</b>
<b>Abstract</b>	<b>III</b>
<b>Sammendrag</b>	<b>V</b>
<b>Table of Contents</b>	<b>VII</b>
<b>List of Tables</b>	<b>IX</b>
<b>List of Figures</b>	<b>IX</b>
<b>List of Symbols</b>	<b>XI</b>
<b>1 Introduction</b>	<b>1</b>
<b>2 Model formulation</b>	<b>3</b>
2.1 Description of the system . . . . .	3
2.2 Definition of the droplet density function . . . . .	4
2.3 Formulation of the population balance . . . . .	5
2.4 Moving interface . . . . .	6
2.5 Coalescence rate closure relationship . . . . .	7
2.5.1 Collision frequency . . . . .	8
2.5.2 Coalescence efficiency . . . . .	9
2.5.3 Interfacial coalescence rate . . . . .	9
2.6 Dimensional analysis of the model . . . . .	9
2.7 Dimensionless population balance . . . . .	11
2.8 Numerical Solution . . . . .	13
<b>3 Parameter estimation</b>	<b>15</b>
<b>4 Experimental</b>	<b>17</b>
<b>5 Results</b>	<b>19</b>
5.1 0/100 . . . . .	19
5.2 25/75 . . . . .	22
5.3 50/50 . . . . .	25
5.4 75/25 . . . . .	28
5.5 100-0 . . . . .	31
5.6 Comparison . . . . .	34
<b>6 Conclusion</b>	<b>37</b>
<b>7 Bibliography</b>	<b>39</b>



## List of Tables

1	Fitting parameters . . . . .	15
2	System specification . . . . .	16
3	The different ratios of demulsifiers that were testes . . . . .	17
4	Fitting parameters for 0-100, Pure Demulsifier 2 . . . . .	19
5	Fitting parameters for 25-75, Demulsifier 1 and Demulsifier 2 . . . . .	22
6	Fitting parameters for 50-50, Demulsifier 1 and Demulsifier 2 . . . . .	25
7	Fitting parameters for 75-25, Demulsifier 1 and Demulsifier 2 . . . . .	28
8	Fitting parameters for 100-0, Pure Demulsifier 1 . . . . .	31
9	Comparison of the $U_{f,max}$ and $R_{g,max}$ for each of the cases . . . . .	34
10	Comparison of the initial mean radii and standard deviation for each of the cases . . . . .	34

## List of Figures

1	Sedimentation in a batch gravity separator . . . . .	3
2	Initial Distribution 0-100 . . . . .	19
3	Separation Profile 0-100 . . . . .	20
4	General Contours 0-100 . . . . .	20
5	Continuous phase velocity profile 0-100 . . . . .	21
6	Initial Distribution 25-75 . . . . .	22
7	Separation Profile 25-75 . . . . .	23
8	General Contours 25-75 . . . . .	23
9	Continuous phase velocity profile 25-75 . . . . .	24
10	Initial Distribution 50-50 . . . . .	25
11	Separation Profile 50-50 . . . . .	26
12	General Contours 50-50 . . . . .	26
13	Continuous phase velocity profile 50-50 . . . . .	27
14	Initial Distribution 75-25 . . . . .	28
15	Separation Profile 75-25 . . . . .	29
16	General Contours 75-25 . . . . .	29
17	Continuous phase velocity profile 75-25 . . . . .	30
18	Initial Distribution 100-0 . . . . .	31
19	Separation Profile 100-0 . . . . .	32
20	General Contours 100-0 . . . . .	32
21	Continuous phase velocity profile 100-0 . . . . .	33





## List of Symbols

$\Delta r$	Difference between the maximum and minimum drop radius	$m$
$\Gamma$	Equilibrium adsorption isotherm	$mol/m^2$
$\gamma$	Interfacial tension	$N/m$
$\Gamma_\infty$	Maximum adsorption phase concentration	$mol/m^2$
$\kappa_{CE}$	Dimensionless coalescence efficiency parameter	—
$\kappa_{CR}$	Dimensionless collision rate parameter	—
$\kappa_{IC}$	Dimensionless interfacial coalescence rate parameter	—
$\kappa_{Pe}$	Dimensionless droplet pair Pecklet number parameter	—
$\lambda$	Dimensionless axial coordinate of the settler	—
$\mu_c$	Viscosity of the continuous phase	$N * s/m^2$
$\mu_r$	Mean droplet radius of the emulsion at any given position and time in the settler	$m^3$
$\Omega$	Domain of the subscripted independent variable	—
$\omega$	Watercut of the emulsion	—
$\omega_{cB}$	Component of the binary droplet collision rate function resulting from Brownian motion	$m^3/s$
$\omega_{cG}$	Component of the binary droplet collision rate function resulting from differential sedimentation	$m^3/s$
$\omega_c$	Binary droplet collision rate function	$m^3/s$
$\phi$	Local volume fraction of droplets	—
$\psi_c$	Binary droplet coalescence efficiency function	—
$\rho_c$	Mass density of the continuous phase of emulsion	$kg/m^3$
$\rho_d$	Mass density of the disperse phase of the emulsion	$kg/m^3$
$\sigma_v$	Standard deviation of the droplet radius	$m^3$
$\tau$	Dimensionless time variable	—
$\tau_c$	Characteristic coalescence time	—
$\Upsilon_\lambda$	Dimensionless sedimentation velocity function	—
$\xi$	Dimensionless drop radius coordinate	—
$A_{CS}$	Cross section area of gravity settler	$m^2$
$B$	Intermolecular force coefficient at the phase interface	$N * m^2$
$C$	Surfactant concentration	—
$C_S$	Concentration of a surface active molecule in the bulk continuous phase of the emulsion	$mol/m^3$
$D_{RR'}$	Relative rate of diffusion between a droplet having a radius R and a droplet having R'	$m^2/s$
$D_s$	Surfactant diffusion coefficient	$m^2/s$
$F$	Squeezing force on a coalescing droplet	$N$
$f$	Dimensionless average number density function	—
$g_z$	Component of acceleration due to gravity in the axial z direction	$m/s^2$
$H$	Height of the total liquid volume in the gravity settler	$m$
$H_i$	Height of the resolved dispersed phase layer	$m$
$K_A$	Langmuir constant	$m^3/mol$
$k_b$	Boltzmann constant	$J/K$
$k_{CE}$	Empirical fitting parameter for the binary coalescence efficiency	$s$
$k_{CR}$	Empirical fitting parameter for the collision rate	—
$k_{IC}$	Empirical fitting parameter for the interfacial coalescence time	—
$k_{SV}$	Empirical fitting parameter for the hindered sedimentation function	—
$N$	Number of phase droplets per unit volume of physical space, referred to as number density	$m^{-3}$
$n$	Average number of disperse phase droplets per unit volume of internal and external state space	$m^{-4}$
$P_b$	Dimensionless droplet birth rate due to binary coalescence	—
$P_d$	Dimensionless droplet death rate due to binary coalescence	—
$P_i$	Dimensionless droplet death rate due to interfacial coalescence	—
$Pe$	Droplet pair Pecklet number based on the droplet volume	—
$Pe_{RR'}$	Droplet pair Pecklet number based on the droplet radius	—
$r$	External droplet state coordinate vector	—
$R_b$	Rate of birth of droplets due to binary coalescence per unit volume of internal and external droplet radius	$m^{-4} * s^{-1}$
$r_c$	Binary coalescence frequency	$m^3/s$
$R_d$	Rate of death of droplets due to binary coalescence per unit volume of internal and external droplet radius	$m^{-4} * s^{-1}$

$R_{g,z}$	Drop growth rate	—
$r_{max}$	Maximum droplet radius considered in the model	$m$
$r_{min}$	Minimum droplet radius considered in the model	$m$
$T$	Absolute temperature	$K$
$t$	Time coordinate	$s$
$t_{bc}$	Binary film drainage and rupture time	$s$
$t_c$	General expression for film drainage and rupture time	$s$
$t_{ic}$	Interfacial film drainage and rupture time	$s$
$U_c$	Sedimentation velocity of a droplet having the characteristic volume, $V_c$	$m/s$
$U_{f,z}$	Continuous phase velocity	—
$U_{ic}$	Interfacial coalescence velocity	$m/s$
$U_{RR'}$	Relative sedimentation velocity between a droplet having a radius $R$ and a radius $R'$	$m/s$
$U_z$	Component of the sedimentation velocity of a droplet in the axial $z$ direction of the settler	$m/s$
$V$	Total volume of the liquid in the settler	$m^3$
$v$	Volume droplet coordinator	$m^3$
$x$	External droplet state coordinate vector	—
$z$	Axial coordinate for the settler	$m$

## 1 Introduction

Dispersions of liquid-liquid colloidal systems influenced by gravity are widespread in many industries, such as the chemical, food, hydro-metallurgical or petroleum industry. In the petroleum industry this is a very crucial process, especially regarding the oil-water emulsions [12]. This makes it an important field to develop a more thorough understanding on how this complex system works. Another reason is that the current mature oilfields contain heavier oils and in order to extract more oil, further research is needed. There has been a lot of research on large scale oil-water separation but very little that mechanically accounts for the poly-dispersity of the emulsion drop-size distribution.

This report focuses on comparing the given model with different experimental results to observe which chemicals provide the fastest/best separation of an oil emulsion. An important aspect with this report was to make a distinction between the sedimentation and coalescence with dynamic and spatial evolution of the droplet size distribution. Calculating the volume rate of sedimentation and the volume rate of coalescence help distinct the behaviour of the separation in each of the cases.

Numerous separation models have been developed over the years [6, 7, 11, 10, 8, 3]. The models of Jeelani and Hartland for the continuous separation of liquid/liquid dispersions consider the binary and interfacial coalescence of drops. Those models estimate the variation in dispersion height, flow and droplet velocity in a batch horizontal settler. In later reports they elucidated the effect of dispersion phase holdup at different dispersion heights, with varying sedimentation heights and coalescing interfaces with time [10]. Some models take into consideration the droplet deformation [8], but since for crude oil emulsions the mean droplet diameter is much smaller than for other chemical processes (a few  $\mu\text{m}$  compared to few hundreds of  $\mu\text{m}$ ) in most cases, taking the droplet deformation into account is not necessary [16]. In this case, the dispersed droplets can be considered as rigid spheres.

It is important to point out here, that the models described above, only consider uniform drop size distributions at any local height in the column. However, due to the fact that in a batch gravity separator, droplet collisions occur mainly due to the differential sedimentation of unequal size drops [2], there is a significant drawback to using uniform dropsize models with respect to determining the real coalescence rate and mechanistic behavior of the emulsion separation process. A population balance [17, 4] on the other hand considers nonuniform drops and has coalescence occurring by simultaneous collisions and film drainage during the time of contact. The interfacial coalescence is modelled on the basis of film drainage models. The film drainage rate is obtained by a parallel film drainage model that combines the squeezing force and a retarded Hamaker constant which represents the mutual attraction forces of the fluid molecules on both sides of the liquid film [9]. A key aspect that combines the physical properties of the bulk fluids, liquid-liquid interface, the effects of surface properties in the interfacial phase as well as the squeezing force of the dense packed layer is the film drainage rate. As the droplets are frequently in contact with each other the limiting factor for coalescence is the film drainage time [8]. The film drainage time is defined as the time from when the approaching droplet decelerates at the interface to time when the interfacial film ruptures in other words, as the film is thinning.

The population balance model allows one to observe how the droplet growth rate, mean droplet radius and the standard deviation, of the droplet size distribution evolve over time at any axial position in the separator, when you have a non-uniform distribution everywhere.

Typically a water in crude oil needs to be separated. In order to to separate these two phases the droplets of the dispersed phase must grow in size to be able to settle from gravitational forces. The gathering of droplets which results in larger droplets is coalescence. For crude oils the drop growth (coalescence) is usually promoted with the addition of the chemical demulsifiers.

In this work, the approach was to model experimental NMR data with the population balance. This was performed in order to determine the chemicals' effect on the sedimentation and coalescence sub-processes. The maximum continuous phase velocity and the maximum drop growth rate estimate the behavior of the separation, if the separation has fast individual separation and/or fast binary coalescences. This model takes this film drainage model together with a population balance model, and experimentally measured poly dispersed initial drop size distribution into to simulate the separation of this water in oil emulsion.

## 2 Model formulation

This model is based on mathematical formulation from previous articles provided by Ugelstad Laboratory, [4],[5].

The model is based on this gravity batch system see Figure 1.

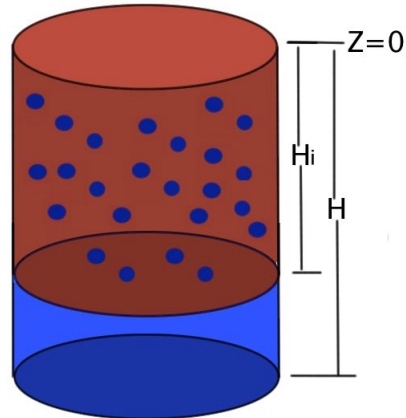


Figure 1: Sedimentation in a batch gravity separator

### 2.1 Description of the system

The interface of the resolved dispersed phase changes with time due to the interfacial coalescence. The small droplets coalesce over time thus droplets increase in size. In this W/O case, the water droplets settle at the bottom. The watercut ( $\omega$ ) is based on that whether the oil or water is continuous phase in the emulsion the volume fraction ( $\phi_0$ ) can be determined.  $\phi$  - volume fraction of dispersed phase. Equation (1) is regarding the water in oil emulsion. while Equation (2) is for oil in water emulsion.

$$\phi_0 = \omega \quad (1)$$

$$\phi_0 = 1 - \omega \quad (2)$$

$H_i$  - for an sedimentation system is measured from the top down to the phase shift, sets  $z=0$  at top of the cylinder.

$$H_i = H_i(t) \quad (3)$$

## 2.2 Definition of the droplet density function

In order to get a good overview of the population density, a few factors have to be taken into consideration.

$n$  - average number of disperse phase droplets per unit volume of internal and external droplet state space [ $1/m^4$ ]

$$n \equiv n(r, z, t) \quad \Omega_t \equiv [0, t], \Omega_r \equiv [r_{min}, r_{max}], \Omega_z \equiv [0, H_i(t)] \quad (4)$$

$N$  - number of disperse phase droplets per unit volume of physical space number density [ $1/m^3$ ]

$$N(z, t) = \int_{r_{min}}^{r_{max}} n(r', z, t) dr' \quad \Omega_t \equiv [0, t], \Omega_z \equiv [0, H_i(t)] \quad (5)$$

$\phi$  - local volume fraction of droplets

$$\phi(z, t) = \int_{r_{min}}^{r_{max}} \left( \frac{4}{3} \pi r'^3 \right) n(r', z, t) dr' \quad \Omega_t \equiv [0, t], \Omega_z \equiv [0, H_i(t)] \quad (6)$$

$\mu_r$  - the mean droplet radius of emulsion at any given term

$$\mu_r = \frac{1}{\phi(z, t)} \int_{r_{min}}^{r_{max}} \left( \frac{4}{3} \pi r'^3 \right) r' n(r', z, t) dr' \quad \Omega_t \equiv [0, t], \Omega_z \equiv [0, H_i(t)] \quad (7)$$

$\sigma_r$  - Standard deviation of the droplet radius of the emulsion at any given position and time in the settler

$$\sigma_r^2(z, t) = \frac{1}{\phi(z, t)} \int_{r_{min}}^{r_{max}} (r'^3 - \mu_r(z, t))^2 \frac{4\pi}{3} r'^3 n(r', z, t) dr' \quad (8)$$

$n$  is considered to be uniform along axial direction ( $z$ ) of the column at  $t=0$ , thus we can define the initial conditions as follows:

$$n_0 \equiv n_0(r) \quad \Omega_r \equiv [r_{min}, r_{max}] \quad (9)$$

$$N_0 = \int_{r_{min}}^{r_{max}} n_0(r') dr' \quad (10)$$

$$\phi_0 = \int_{r_{min}}^{r_{max}} \frac{4}{3} \pi r'^3 n_0(r') dr' \quad (11)$$

$$\mu_{r_0} = \frac{1}{\phi_0} \int_{r_{min}}^{r_{max}} \frac{4}{3} \pi r'^3 r' n_0(r') dr' \quad (12)$$

$$\sigma_{r_0}^2 = \frac{1}{\phi_0} \int_{r_{min}}^{r_{max}} (r' - \mu_{r_0})^2 \frac{4}{3} \pi r'^3 n_0(r') dr' \quad (13)$$

### 2.3 Formulation of the population balance

Here it is defined what goes in and what goes out, or birth and death of droplets, as well as the sedimentation velocity.

The velocity of the droplets can be represented by the sedimentation velocity,  $U_z$ , [13]

$$U_z(r, z, t) = \left[ \frac{2(\rho_d - \rho_c)g_z r^2}{9\mu_c} \right] [1 - \phi(z, t)]^{k_{sv}} \quad (14)$$

$$\Omega_t \equiv [0, t], \Omega_r \equiv [r_{min}, r_{max}], \Omega_z \equiv [0, H_i(t)]$$

Equation (14) comes from a combination of stokes law and and stokes law for terminal velocity of a sphere falling in fluids as demonstrated in Equation (15)

$$\begin{aligned} F_d &= 6\pi\mu R U_z \\ F_g &= (\rho_p - \rho_f)g \frac{4}{3}\pi R^3 \\ V &= \frac{4\pi}{3}R^3 \implies R = \left( V \frac{3}{4\pi} \right)^{1/3} \\ F_d &= F_g \\ 6\pi\mu R U_z &= (\rho_p - \rho_f)g \frac{4}{3}\pi R^3 \\ \text{Solve with regards to } U_z & \\ U_z &= \underbrace{\left( \frac{3}{4\pi} \right)^{2/3} 2(\rho_p - \rho_f)g 9\mu V^{2/3}}_{\text{result of Stokes law}} \underbrace{[1 - \phi(z, t)]^{k_{sv}}}_{\text{Hindered sedimentation}} \end{aligned} \quad (15)$$

The droplet death rate  $R_d$  and the droplet birth rate  $R_b$  is given in Equation 17 and 16, respectively.

$$R_b(r, z, t) = \int_{r_{min}}^{\frac{r}{2\sqrt{3}}} r_c([r^3 - r'^3]^{1/3}, r', z, t) n([r^3 - r'^3]^{1/3}, z, t) n(r', z, t) dr' \quad (16)$$

$$\Omega_t \equiv [0, t], \Omega_r \equiv [r_{min}, r_{max}], \Omega_z \equiv [0, H_i(t)]$$

$$R_d(r, z, t) = n(r, z, t) \int_{r_{min}}^{r_{max}} r_c(r, r', z, t) n(r', z, t) dr' \quad (17)$$

$$\Omega_t \equiv [0, t], \Omega_r \equiv [r_{min}, r_{max}], \Omega_z \equiv [0, H_i(t)]$$

Population balance is given in Equation (18), with initial conditions shown in Equation (19) and boundary conditions, Equation (20). The effective diffusion due to compressive stress ( $D_{CS}$ ) is used in the population balance.

$$\frac{\partial n(r, z, t)}{\partial t} + \frac{\partial}{\partial z}[U_z(r, z, t)n(r, z, t)] + R_d(r, z, t) - R_b(r, z, t) - r^2 D_{CS} \frac{\partial^2 n(r, z, t)}{\partial z^2} = 0 \quad (18)$$

$$\Omega_t \equiv [0, t], \Omega_r \equiv [r_{min}, r_{max}], \Omega_z \equiv [0, H_i(t)]$$

Initial conditions

$$n(r, 0, t) = n_0(r), \Omega_r \equiv [r_{min}, r_{max}], \Omega_z \equiv [0, H_i(t)] \quad (19)$$

Boundary conditions

$$n(r, 0, t) = 0, \Omega_t \equiv [0, t], \Omega_r \equiv [r_{min}, r_{max}] \quad (20)$$

## 2.4 Moving interface

In order to observe how the  $H_i(t)$  moves with time, redefine an interfacial coalescence velocity  $U_{ic}$

$$U_{ic} = \frac{r}{3t_{ic}} \quad (21)$$

Where  $t_{ic}$  is the interfacial coalescence time and is defined below. Based on this definition of  $U_{ic}$ , the height of the resolved dispersed phase interface can be defined as follows:

$$\frac{\partial H_i}{\partial t} = \frac{-1}{1 - \phi(H_i, t)} \int_{r_{min}}^{r_{max}} U_{ic} \left( \frac{4\pi}{3} r'^3 \right) n(r', H_i, t) dr' \quad (22)$$

Initial condition for the  $H_i$  is given by the following:

$$H_i(0) = H \quad (23)$$



## 2.5 Coalescence rate closure relationship

Need to specify the binary coalescence rate function ( $r_c$ ) and the interfacial coalescence time. The binary coalescence rate function is the product of the collision frequency function  $\omega_c$  and the coalescence efficiency function  $\psi_e$ .

$$r_c(r, r', z, t) = \omega_c(r, r', z, t)\psi_e(r, r', z, t) \quad (24)$$

$$\Omega_t \equiv [0, t], \Omega_r \equiv [r_{min}, r_{max}], \Omega_z \equiv [0, H_i(t)]$$

The film drainage rate between the drops can be estimated with the results of the parallel film drainage model,[15]. In Equation (25) the coalescence time is the result of this film drainage model. This equation combines the squeezing force on the droplets (F), and the intermolecular forces at the phase interface (Hamaker constant, B). This function combines the physical properties of the; bulk fluids, liquid-liquid interphase, the effects of surface properties in the interface phase as well as the squeezing force of the dense packed layer, this results in the film drainage time shown in Equation (25). However this film drainage model is only viable if the the initial radii of the dispersed phase droplets are small compared to the continuous phase, which it is in this case. If larger drops are present a model that includes the dimpled formation on the droplet should be included. The dimpled deformation is a nonuniform thickness of the film, caused by the Marangoni effect (an surface tension gradient). General droplet deformation should also be included for larger droplets, larger droplets would affect the coalescence behavior [3].

$$t_c = 1.046 \frac{3\sqrt{\pi}\mu_c R_f^3}{4\sqrt{FB}} \quad (25)$$

### 2.5.1 Collision frequency

The sphere pair Pecklet number ( $Pe_{RR'}$ ) is an result for colliding spheres by combining both diffusive and convective fluxes [14].

$$Pe_{RR'}(z, t) = \frac{(R + R')U_{RR'}(z, t)}{D_{RR'}} \quad (26)$$

Where the relative sedimentation velocity are as follows:

$$U_{RR'}(z, t) = \frac{2(\rho_d - \rho_c)g_z}{9\mu_c} [1 - \phi(z, t)]^{k_{sv}} |R^2 - R'^2| \quad (27)$$

And the relative rate of diffusion between droplets are:

$$D_{RR'} = \frac{k_B T}{6\pi\mu_c} \left[ \frac{R + R'}{RR'} \right] \quad (28)$$

By inserting Equation (27) and Equation (28) in Equation (26), this results in Equation (29).

$$Pe_{RR'} = \frac{4\pi(\rho_d - \rho_c)g_z}{3k_B T} [1 - \phi(z, t)]^{k_{sv}} RR' |R^2 - R'^2| \quad (29)$$

The collision rate  $\omega_c$  expressed as follows

$$\omega_c(R, R', z, t) = \omega_{cB}(R, R') + \omega_{cG}(R, R', z, t) [1 + 4.496(Pe_{RR'}(z, t))^{-2/3}] \quad (30)$$

$$\omega_{cB}(R, R') = 4\pi(R + R')D_{RR'} \quad (31)$$

$$\omega_{cG}(R, R', z, t) = \pi(R + R')^2 U_{RR'}(z, t) \quad (32)$$

After substitution and rearrangement of the above equations, and adding an empirical scaling factor,  $k_{CR}$  you get an function of  $\omega_c$  that is dependent on  $r, r', z, t$ .

$$\omega_c(r, r', z, t) = k_{CR} \frac{k_B T}{6\mu_c} \frac{(r + r')^2}{rr'} [1 + Pe(r, r', z, t) + 4.496(Pe(r, r', z, t))^{1/3}] \quad (33)$$

$$\Omega_t \equiv [0, t], \Omega_r \equiv [r_{min}, r_{max}], \Omega_z \equiv [0, H_i(t)]$$

$$Pe(r, r', z, t) = \frac{(\rho_d - \rho_c)g_z}{k_B T} (1 - \phi(z, t))^{k_{sv}} rr'^{1/3} |r^2 - r'^2| \quad (34)$$

$$\Omega_t \equiv [0, t], \Omega_r \equiv [r_{min}, r_{max}], \Omega_z \equiv [0, H_i(t)]$$

### 2.5.2 Coalescence efficiency

The binary droplet coalescence efficiency function ( $\psi_e$ ), given in Equation (36) this is a function that is defined as the ratio between binary coalescence time ( $t_{bc}$ , Equation (35)) and contact time. This contact time is given as a fitting parameter,  $k_{CE}$ .

$$t_{bc}(r, r', z, t) = 1.046 \frac{\mu_c(\rho_d - \rho_c)gz}{\gamma(C_s(z, t))^{3/2} B(C_s(z, t))^{1/2}} \left[ \frac{rr'}{r+r'} \right]^{9/2} \quad (35)$$

$$\psi_e(r, r', z, t) = \exp \left[ -\frac{1}{k_{CE}} t_{bc}(r, r', z, t) \frac{|U(r) - U(r')|}{|r+r'|} \right] \quad (36)$$

$$\Omega_t \equiv [0, t], \Omega_r \equiv [r_{min}, r_{max}], \Omega_z \equiv [0, H_i(t)]$$

### 2.5.3 Interfacial coalescence rate

The interfacial coalescence rate is obtained by combining Equation (35) with a limit of  $r' \rightarrow 0$  and a new fitting parameter,  $k_{IC}$ .

$$t_{ic}(r, t) = \frac{1.046}{k_{IC}} \frac{\mu_c(\rho_d - \rho_c)gz}{\gamma(C_s(H_i(t), t))^{3/2} B(C_s(H_i(t), t))^{1/2}} r^{9/2} \quad (37)$$

$$\Omega_t \equiv [0, t], \Omega_r \equiv [r_{min}, r_{max}]$$

## 2.6 Dimensional analysis of the model

Within this section there will be defined new dimensionless- velocity, time and length functions, this is for easier scaling of the model.

$U_c$  - Velocity

$$U_c = \frac{2(\rho_d - \rho_c)gz}{9\mu_c} r_c^2 \quad (38)$$

$\tau$  - Dimensionless time

$$\tau = \frac{U_c}{H} t \quad (39)$$

$\lambda$  - Dimensionless axial direction (time dependent)

$$\lambda = \frac{z}{H_i} = \frac{z}{H\Theta} \quad (40)$$

$\xi$  - Dimensionless drop radius coordinate

$$\xi = \frac{r - r_{min}}{\Delta r} \quad (41)$$

$$\Delta r = r_{max} - r_{min} \quad (42)$$

$\Theta$  - Dimensionless value of the position of the resolved waterphase

$$\Theta = \frac{H_i}{H} \quad (43)$$

$f$  - Dimensionless average number density

$$f = \frac{\Delta r}{N_0} n \quad (44)$$

$Y_\lambda$  - Dimensionless sedimentation velocity

$$Y_\lambda = \frac{U_z}{U_c} \quad (45)$$

Want to express any function of the time derivative  $\partial/\partial t$  as a directional derivative in  $\lambda - \tau$  -space, Equations (46) to (50).

$$\frac{\partial n}{\partial t} = \left( \frac{\partial \tau}{\partial t} \right) \frac{\partial n}{\partial \tau} + \left( \frac{\partial \lambda}{\partial t} \right) \frac{\partial n}{\partial \lambda} \quad (46)$$

$$\frac{\partial}{\partial z}(U_z n) = \left( \frac{\partial \lambda}{\partial z} \right) \frac{\partial}{\partial \lambda}(U_z n) \quad (47)$$

$$\frac{\partial \tau}{\partial t} = \frac{U_c}{H} \quad (48)$$

$$\frac{\partial \lambda}{\partial t} = \left( \frac{\partial \tau}{\partial t} \right) \frac{\partial \lambda}{\partial \tau} = - \left( \frac{U_c}{H} \right) \frac{\lambda}{\Theta} \frac{\partial \Theta}{\partial \tau} \quad (49)$$

$$\frac{\partial \lambda}{\partial z} = \frac{1}{H\Theta} \quad (50)$$

By combining Equation (46)-(50) with Equation (44) and Equation (45) you obtain Equation (51) and Equation (52).

$$\frac{\partial n}{\partial t} = \left( \frac{U_c N_0}{H \Delta v} \right) \frac{\partial f}{\partial \tau} - \left( \frac{U_c N_0}{H \Delta v} \right) \frac{\lambda}{\Theta} \frac{\partial \Theta}{\partial \tau} \frac{\partial f}{\partial \lambda} \quad (51)$$

$$\frac{\partial}{\partial z}(U_z n) = \left( \frac{U_c N_0}{H \Delta v} \right) \frac{1}{\Theta} \frac{\partial}{\partial \lambda}(Y_\lambda f) \quad (52)$$

## 2.7 Dimensionless population balance

By combining Equation (38)-(52) with the population balance, Equation (18), you obtain the dimensionless, scalable population balance, Equation (53).

$$\frac{\partial f(\xi, \lambda, \tau)}{\partial \tau} = \frac{\lambda}{\Theta(\tau)} \frac{d\Theta(\tau)}{d\tau} \frac{\partial f(\xi, \lambda, \tau)}{\partial \lambda} - \frac{Y_\lambda(\xi, \lambda, \tau)}{\Theta(\tau)} \frac{\partial f(\xi, \lambda, \tau)}{\partial \lambda} \quad (53)$$

$$- \frac{f(\xi, \lambda, \tau)}{\Theta(\tau)} \frac{\partial Y_\lambda(\xi, \lambda, \tau)}{\partial \lambda} - P_d(\xi, \lambda, \tau) + P_b(\xi, \lambda, \tau) - P_i(\xi, \lambda, \tau)$$

$$\Omega_\xi \equiv [0, 1], \Omega_\lambda \equiv [0, 1], \Omega_\tau \equiv [0, \tau]$$

$$\frac{\partial \Theta(\tau)}{\partial \tau} = \frac{-\kappa_{IC}}{1 - \phi(1, \tau)} \left( \frac{4\pi N_0}{3 U_c} \right) \int_0^1 \frac{(r_{min} + \Delta r \xi)^3}{t_{ic}} f(\xi', 1, \tau) d\xi' \quad (54)$$

$$\Omega_\tau \equiv [0, \tau]$$

The initial conditions for Equation (53) and Equation (54) is given in Equation (55) and Equation (56), respectively.

$$f(\xi, \lambda, 0) = \frac{\Delta r}{N_0} n_0(\xi) \quad (55)$$

$$\Omega_\xi \equiv [0, 1], \Omega_\lambda \equiv [0, 1]$$

$$\Theta(0) = 1 \quad (56)$$

The boundary condition for Equation (53) is given with Equation (57).

$$f(\xi, 0, \tau) = 0 \quad (57)$$

$$\Omega_\xi \equiv [0, 1], \Omega_\tau \equiv [0, \tau]$$

The normalized velocity is given presented by the function  $\Upsilon$ , and is presented by Equation (58).

$$\Upsilon_\lambda(\xi, \lambda, \tau) = \frac{U_z}{U_c} = \left( \frac{r_{min} + \xi \Delta r}{r_{max}} \right)^2 [1 - \phi(\lambda, t)]^{k_{sv}} \quad (58)$$

$$\Omega_\xi \equiv [0, 1], \Omega_\tau \equiv [0, \tau], \Omega_\lambda \equiv [0, 1]$$

The volume fraction of the dispersed phase as a function of dimensionless variables  $(\xi, \lambda, \tau)$  is given with Equation (59).

$$\phi(\lambda, \tau) = N_0 \Delta r \int_0^1 \left( \frac{r_{min}}{\Delta r} + \xi' \right)^3 f(\xi', \lambda, \tau) d\xi' \quad (59)$$

$$\Omega_\tau \equiv [0, \tau], \Omega_\lambda \equiv [0, 1]$$

Equation (60) Gives the ratio between the systems time constant and the coalescence time ( $\tau_C$ , given in Equation (61), this time ratio is scaled with a fitting constant  $k_{IC}$ .

$$\kappa_{IC}(\tau) = \frac{k_{IC}H}{\tau_C(1,\tau)U_C} = \frac{k_{IC}\gamma(1,\tau)^{3/2}B(1,\tau)^{1/2}}{1,046\mu_c(\rho_d - \rho_c)g_z} \frac{H}{U_C} (r_{max})^2 \quad (60)$$

$$\Omega_\tau \equiv [0, \tau]$$

Coalescence time,  $\tau_C$ .

$$\tau_C(\lambda, \tau) = 1.046 \frac{\mu_c(\rho_d - \rho_c)g_z(r_{max})^2}{\gamma(\lambda, \tau)^{3/2}B(\lambda, \tau)^{1/2}} \quad (61)$$

$$\Omega_\tau \equiv [0, \tau], \Omega_\lambda \equiv [0, 1]$$

$P_i$  is the rate of droplet consumption that occurs because of interfacial coalescence, given in Equation (62).

$$P_i(\xi, \lambda, \tau) = \kappa_{IC}(\tau)u(\lambda - 1)f(\xi, \lambda, \tau) \left( \frac{r_{min}}{\Delta r} + \xi \right)^{-3/2} \quad (62)$$

$$\Omega_\xi \equiv [0, 1], \Omega_\tau \equiv [0, \tau], \Omega_\lambda \equiv [0, 1]$$

$\alpha$  expresses the upper integral limits of the birth/death rate of the droplets.

$$\alpha = \frac{r - r_{min}}{\xi_{UL}\Delta r} \quad (63)$$

The birth- ( $P_b$ ) and death- ( $P_d$ ) -rate are given presented in dimensionless form in Equation (64) and Equation (65).

$$P_b(\xi, \lambda, \tau) = \kappa_{CR} \frac{\xi}{2(1 - \phi(\lambda, \tau))} \int_0^1 P_C(\xi_{UL} = \xi, 1 - \alpha', \alpha', \lambda, \tau) f(1 - \alpha', \lambda, \tau) f(\alpha', \lambda, \tau) d\alpha' \quad (64)$$

$$\Omega_\xi \equiv [0, 1], \Omega_\tau \equiv [0, \tau], \Omega_\lambda \equiv [0, 1]$$

$$P_d(\xi, \lambda, \tau) = \kappa_{CR} \frac{f(\xi, \lambda, \tau)}{(1 - \phi(\lambda, \tau))} \int_0^1 P_C(\xi_{UL} = 1, \xi, \alpha', \lambda, \tau) f(\alpha', \lambda, \tau) d\alpha' \quad (65)$$

$$\Omega_\xi \equiv [0, 1], \Omega_\tau \equiv [0, \tau], \Omega_\lambda \equiv [0, 1]$$

$\kappa_{CR}$  - Is the parameter that indicates the amount of droplet that collide due to the brownian motion in the given time constant of the system. This parameter is scaled by the fitting parameter  $k_{CR}$ .

$$\kappa_{CR} = k_{CR} \left( \frac{k_B T N_0}{6\mu_C} \frac{H}{U_C} \right) \quad (66)$$

$P_C$  - Is the coalescence rate in its dimensionless form.

$$P_C(\xi_{UL}, \alpha, \alpha', \lambda, \tau) = \bar{\omega}_C(\xi_{UL}, \alpha, \alpha', \lambda, \tau) \bar{\psi}_e(\xi_{UL}, \alpha, \alpha', \lambda, \tau) \quad (67)$$

$$\Omega_\alpha \equiv [0, 1], \Omega_\tau \equiv [0, \tau], \Omega_\lambda \equiv [0, 1]$$

Equation (68) gives the dimensionless binary droplet coalescence efficiency function.

$$\bar{\psi}_e(\xi_{UL}, \alpha, \alpha', \lambda, \tau) = \exp \left[ -\kappa_{CE}(\lambda, \tau) \xi_{UL}^{3/2} \left( \frac{\left( \frac{r_{min}}{\xi_{UL} \Delta r} + \alpha \right) \left( \frac{r_{min}}{\xi_{UL} \Delta r} + \alpha' \right)}{\left( \frac{r_{min}}{\xi_{UL} \Delta r} + \alpha \right) + \left( \frac{r_{min}}{\xi_{UL} \Delta r} + \alpha' \right)} \right)^{9/2} \right] \quad (68)$$

$$\Omega_\alpha \equiv [0, 1], \Omega_\tau \equiv [0, \tau], \Omega_\lambda \equiv [0, 1]$$

Equation (69) Is the dimensionless coalescence efficiency parameter scaled by the fitting parameter  $\kappa_{CE}$ .

$$\kappa_{CE} = \frac{\tau_C(\lambda, \tau)}{k_{CE}} \quad (69)$$

$$\Omega_\tau \equiv [0, \tau], \Omega_\lambda \equiv [0, 1]$$

$\bar{\omega}_C$ - Is the dimensionless binary droplet coalescence rate function.

$$\bar{\omega}_C(\xi_{UL}, \alpha, \alpha', \lambda, \tau) = \frac{\left( \left( \frac{r_{min}}{\xi_{UL} \Delta r} + \alpha \right) \left( \frac{r_{min}}{\xi_{UL} \Delta r} + \alpha' \right) \right)^2}{\left( \frac{r_{min}}{\xi_{UL} \Delta r} + \alpha \right) + \left( \frac{r_{min}}{\xi_{UL} \Delta r} + \alpha' \right)} \quad (70)$$

$$\times \left[ 1 + Pe(\xi_{UL}, \alpha, \alpha', \lambda, \tau) + 4.496(Pe(\xi_{UL}, \alpha, \alpha', \lambda, \tau))^{1/3} \right]$$

$$\Omega_\alpha \equiv [0, 1], \Omega_\tau \equiv [0, \tau], \Omega_\lambda \equiv [0, 1]$$

This  $Pe(\xi_{UL}, \alpha, \alpha', \lambda, \tau)$  - function is the dimensionless droplet pair Peclet number.

$$Pe(\xi_{UL}, \alpha, \alpha', \lambda, \tau) = \kappa_{PE} \xi_{UL}^{4/3} (1 - \phi(\lambda, \tau))^{k_{sv}} \left( \frac{r_{min}}{\xi_{UL} \Delta r} + \alpha \right) \left( \frac{r_{min}}{\xi_{UL} \Delta r} + \alpha' \right) \quad (71)$$

$$\times \left| \left( \frac{r_{min}}{\xi_{UL} \Delta r} + \alpha \right) - \left( \frac{r_{min}}{\xi_{UL} \Delta r} + \alpha' \right) \right|$$

$$\Omega_\alpha \equiv [0, 1], \Omega_\tau \equiv [0, \tau], \Omega_\lambda \equiv [0, 1]$$

$\kappa_{Pe}$  - Is the dimensionless droplet pair Peclet number.

$$\kappa_{Pe} = \left( \frac{4\pi}{3} \right) \frac{(\rho_d - \rho_c) g_z}{k_B T} \Delta r^4 \quad (72)$$

## 2.8 Numerical Solution

The method used to simulate this combination of equations and also including the experimental data for the initial droplet size distribution were by using orthogonal collocation combined with Gear's backward finite difference algorithm. The purpose for the orthogonal collocation was to transform the partial difference equations to solvable ordinary differential equations. The benefits for using an Orthonormal basis is that it preserves the linear properties of the vectors and also the metric properties. The Gear's backward finite algorithm was used to integrate the equations over time. In order to properly fit the simulated model to the experimental data, the model had to be simulated approximately 15 times for each case. With a simulation time between 6-10 hours this optimization was very time consuming.





### 3 Parameter estimation

In Table 1 the different fitted parameters have been listed along with the initial value and the tested range of values. Testing started with each individual parameter with high values in order to observe the different effect it had on the results. As each experimental comparison had different characteristics it required numerous simulations in order to fit the model properly to the respective case.

**Table 1:** Fitting parameters

Fitting Parameters	Base value	Test range
Collision rate constant, $k_{CR}$	0.25	0.1 - 1.2
Binary coalescence efficiency constant, $k_{CE}$	0.005	0.0005 - 0.05
Interfacial coalescence constant, $k_{IC}$	7	1.0 - 120.0
Effective diffusion due to compressive stress, $D_{CS}$	1.00E+09	1.00E+07 - 1.00E+10

The collision rate constant directly affects the binary droplet collision rate, it is also a factor in scaling the parameter that represents the droplet collisions which greatly affect the birth and death rate, this constant affects equally both birth- and death- rate, it affects the dynamics of the birth/death in the total population balance, see Equation (33).

The binary coalescence efficiency constant is an integral part of a natural exponential function for the binary coalescence efficiency function, so if the constant increases it will affect the coalescence rate, see Equation (36).

The interfacial coalescence constant is directly proportional to the consumption of droplets due to the interfacial coalescence, see Equation (37). The point of this constant is to scale the ratio between the coalescence time of the system to the sedimentation time constant of the system.

The effective diffusion due to compressive stress is used in the population balance, Equation (18), this fitted diffusion constant arises from mechanical equilibrium in the emulsion and is a part of determining the robustness of the model.

It is important to mention that the initial drop size distribution is collected from experimental results along with the volume fraction data for the same experiment. This is the initial dropsize distribution used as the initial condition for the model while total volume fraction data is used to compare the experimental profile of the separation of the emulsion with associated model. Table 2 presents the properties of the experiment, then the same properties were used in the model. The Hamaker constant and the sedimentation constant is only used in the model as a guess. Since measured values of these parameters are not available, thus their true values are lumped into the fitting coefficient.

**Table 2:** System specification

Parameters		
Temperature of the system	60.0	$^{\circ}C$
Water cut (volume fraction of water)	0.41	
Height of the column	$\approx 1.50$	cm*
Radius of the column	0.9	cm
Density of the dispersed phase	983.21	$kg/m^3$
Viscosity of the dispersed phase	0.469	mPa*s
Density of the continuous phase	946.0	$kg/m^3$
Viscosity of the continuous phase	12.0	mPa*s
Surface tension	10.88	mN/m
Retarded Hamaker constant	3.65e-31	$N * m^2$
Sedimentation constant (Empirical fitting parameter)	4.5	

\*not consistent for each experiment, so changed accordingly

## 4 Experimental

The experimental data that was used in the simulation of the model and the values for the initial distribution was obtained from the NMR test results. These test results was from of an emulsion of 60 volume% of "Crude oil B" and 40 volume% of saline (3.5weight% NaCl in  $H_2O$ ) and 100ppm of demulsifier. There were tested a total of 2 demulsifiers, pure demulsifiers and three mixes of the two, with different ratios. The different ratios for each of demulsifier blends are presented in Table 3. The water in oil emulsions were prepared with a Ultra Turrax mixer (IKA, T25 with 10mm head) at 24000rpm for 3 minutes. After the emulsification was complete, the demulsifiers were added to give a concentration of 100ppm in the emulsions, and then shaken to ensure the demulsifiers were dissolved properly in the emulsion. A low field Oxford Instruments Maran Ultra 23 MHz NMR was used to measure the separation profiles of the emulsions. Position-dependent signal of the sample was measured for 120 minutes to obtain the separation profiles. Before measurements the NMR magnet was tempered to the desirable temperature which in these cases were 60 °C [1].

**Table 3:** The different ratios of demulsifiers that were testes

Demulsifier blend ratios	
<u>Demulsifier 1</u>	<u>Demulsifier 2</u>
0	100
25	75
50	50
75	25
100	0

The experimental results were compared to this model. In order to see which chemical mixture that was the best (with the most desirable results), the model was fitted with the optimum fitting parameters for each case to be able to observe the fastest drop growth rate and the maximum sedimentation rate for each experiment. The only way to acquire the optimum parameters were to simulate with different fitting parameters until the model matched the experimental results.



## 5 Results

The NMR results were adapted to fit the simulation program along with its corresponding parameters, then optimized with the different fitting parameters. In this section of the report the results of the simulation are presented for each optimized case. Along with an analysis of these results for all of the five cases. First individual analyses of each of the different demulsifier blends, then a comparison of those blends against each other.

### 5.1 0/100

The fitting parameters used to optimize this separation containing pure demulsifier 2 is presented in table 4.

**Table 4:** Fitting parameters for 0-100, Pure Demulsifier 2

Fitting Parameters	
Collision rate constant, $k_{CR}$	0.25
Binary coalescence efficiency constant, $k_{CE}$	0.005
Interfacial coalescence constant, $k_{IC}$	100
Effective diffusion due to compressive stress, $D_{CS}$	1.00E+09

The initial distribution represents the dimensionless initial density distribution functions (based of volume and average number of disperse phase) as a function of droplet radius, see Figure 2. The red line,  $f_{n0}$ , represents the initial drop number distribution, while the black line,  $f_{v0}$ , represents the initial volume distribution number. The initial drop size distribution are obtained from experimental results. The different fitted parameters have no impact on this distribution. This distribution gives an indication of the separation efficiency in this emulsion, as larger drops initially will separate faster than small droplets.

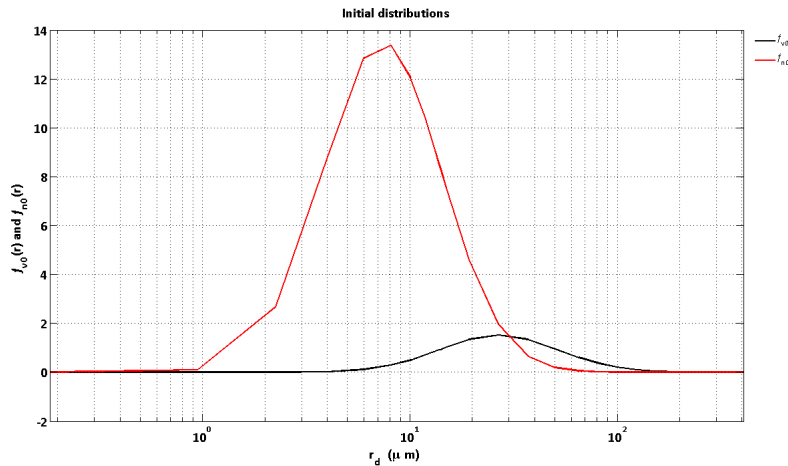


**Figure 2:** Initial Distribution 0-100

In Figure 3, the experimentally measured values of the constant volume fraction levels are represented with different types of dots and the modelled values are represented with the continuous lines. This separation profile demonstrates how the separation along the z-axis develop as a function of time. This separation profile indicates that this is a very rapid as there is a complete

separation occurring at  $\approx 16min$ . The experimental values indicate that the local volume fractions of 0.10 and below never separate, this is most likely due to that the small droplets stick to the glass because of the hydrophilic properties of glass. This tendency is observed for all the separations performed in this report.

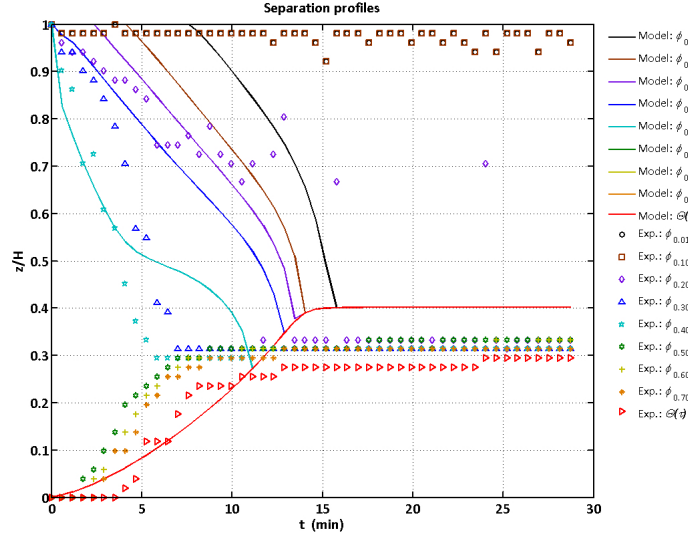


Figure 3: Separation Profile 0-100

In Figure 4, the droplet growth rate, average number density, mean droplet radius and standard deviation of the droplet radius is shown as contour diagrams, with the height ratio as a function of time. It is seen from the droplet growth rate graph that the maximum growth rate occur immediately, and is uniform throughout the height of the column. Logically, as the droplets grow the average number of droplets decrease. The mean droplet radii steadily grows, the drop size is larger at near the bottom of the emulsion, and increase in size as time goes. In under one minute the droplet growth rate has a rapid decline, as the emulsion separate it can be seen that growth rate is largest near the oil water interface.

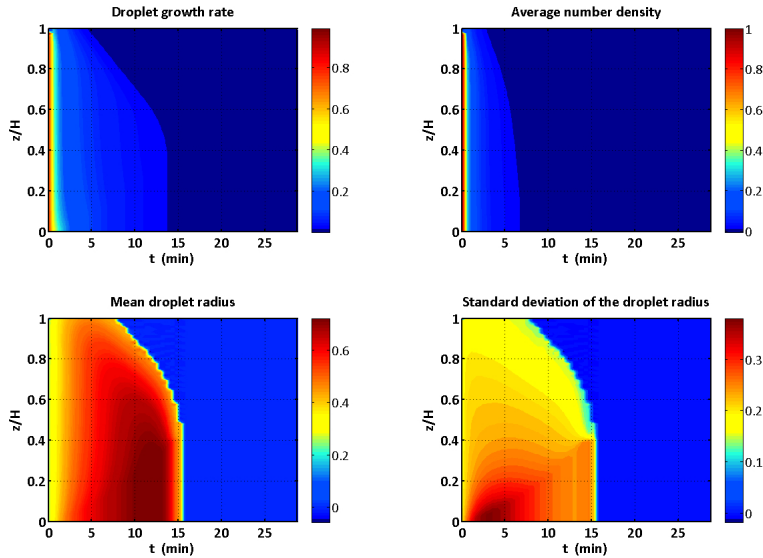


Figure 4: General Contours 0-100

In Figure 5 shows the continuous phase velocity profile as function of the height ratio at different times. The velocity increases with respect to time, this is because as shown in Figure 4 the droplets grow in size as time goes. Large drops create an larger displacement of the continuous phase, and leads to a high velocity of the displaced fluid.

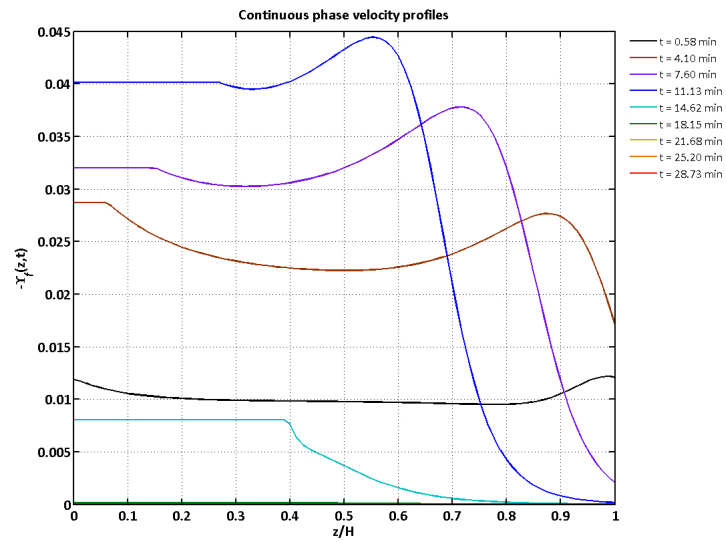


Figure 5: Continuous phase velocity profile 0-100

## 5.2 25/75

The optimized fitting parameters for an emulsion with 25% Demulsifier 1 and 75% Demulsifier 2 are presented in table 5

**Table 5:** Fitting parameters for 25-75, Demulsifier 1 and Demulsifier 2

Fitting Parameters	
Collision rate constant, $k_{CR}$	0.1
Binary coalescence efficiency constant, $k_{CE}$	0.005
Interfacial coalescence constant, $k_{IC}$	15
Effective diffusion due to compressive stress, $D_{CS}$	5.00E+08

In Figure 6. The initial drop size distribution are obtained from experimental results. The distribution of the droplets range from  $0.1\mu m$  to  $10\mu m$  with a majority of droplets at approximately  $1\mu m$  radius.

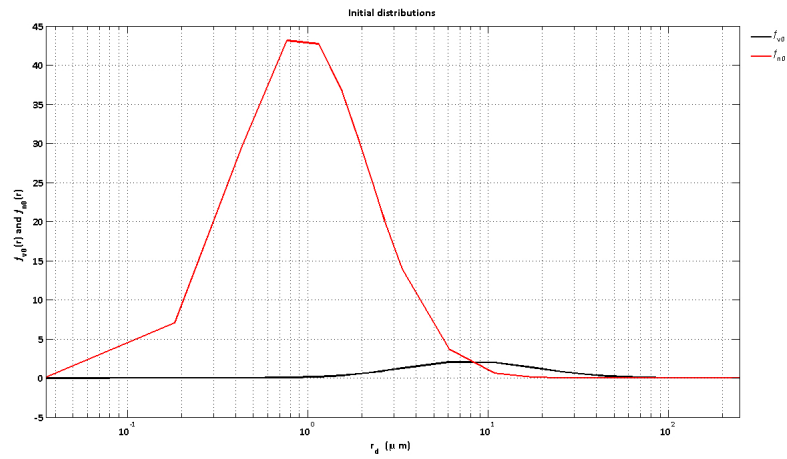


**Figure 6:** Initial Distribution 25-75



In Figure 7, in this separation profile, it can be a rather slow separation. From the experimental values it can seem as the emulsion has a separation of 50% from the start. The lower local volume fractions seem to separate eventually but at slow pace.

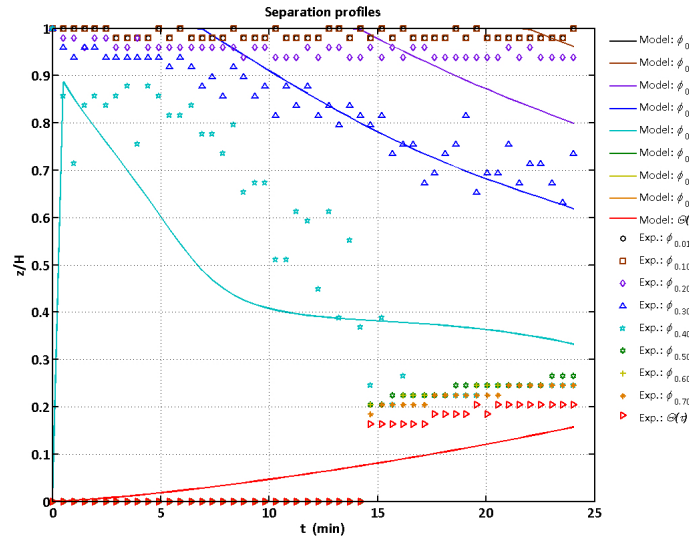


Figure 7: Separation Profile 25-75

In Figure 8, the droplet growth rate, average number density, mean droplet radius and standard deviation of the droplet radius is shown. It is seen from the droplet growth rate graph that the maximum growth rate occur at  $t \approx 0min$ , and is uniform throughout the height of the column. After approximately 1min, the droplet growth rate has a rapid decline, as the emulsion separate it can be seen that growth rate is near the oil water interface. Logically, as the droplets grow the average number of droplets decrease. The mean droplet radius steadily grow, the drop size is larger at near the bottom of the emulsion, and increase in size as time goes.

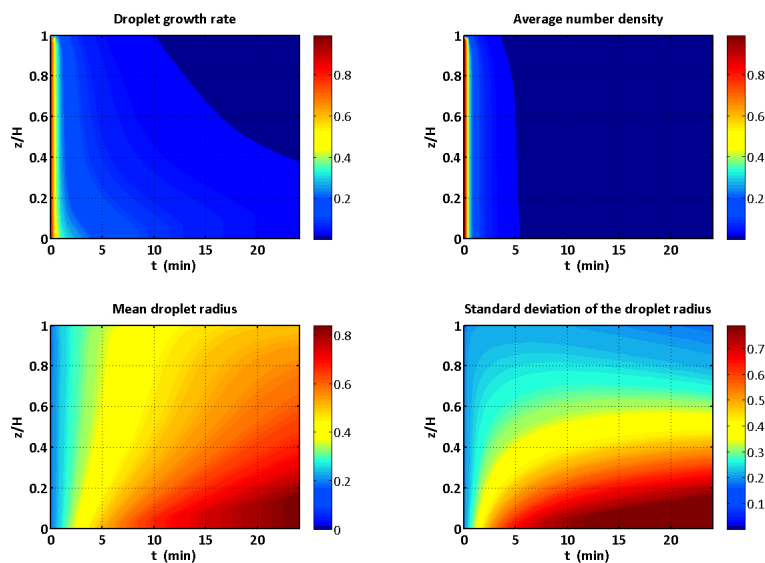


Figure 8: General Contours 25-75

In Figure 9 shows the continuous phase velocity profile as function of the height ratio at different times. The velocity increase with respect to time, this is because as shown in Figure 8 the droplets grow in size as time goes, and larger drops create an larger displacement of the continuous phase, and leads to a high velocity of the displaced fluid

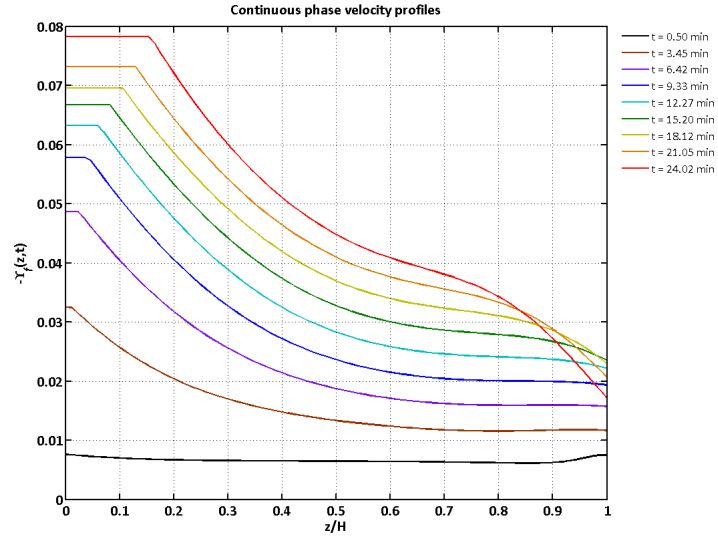


Figure 9: Continuous phase velocity profile 25-75

### 5.3 50/50

The optimized fitted parameters are presented in Table 6. This is for a blend of 50% Demulsifier 1 and Demulsifier 2 with 50/50 mixing ratio, respectively.

**Table 6:** Fitting parameters for 50-50, Demulsifier 1 and Demulsifier 2

Fitting Parameters	
Collision rate constant, $k_{CR}$	1.5
Binary coalescence efficiency constant, $k_{CE}$	0.005
Interfacial coalescence constant, $k_{IC}$	22
Effective diffusion due to compressive stress, $D_{CS}$	5.00E+08

The initial distribution represents the dimensionless initial density distribution functions (Based on Volume and average number of disperse phase) and varies with the droplet radius, see Figure 10 as mentioned before the different fitted parameters have no impact on this distribution. Similar number distribution as for the other blends, only with a lower peak than the others.

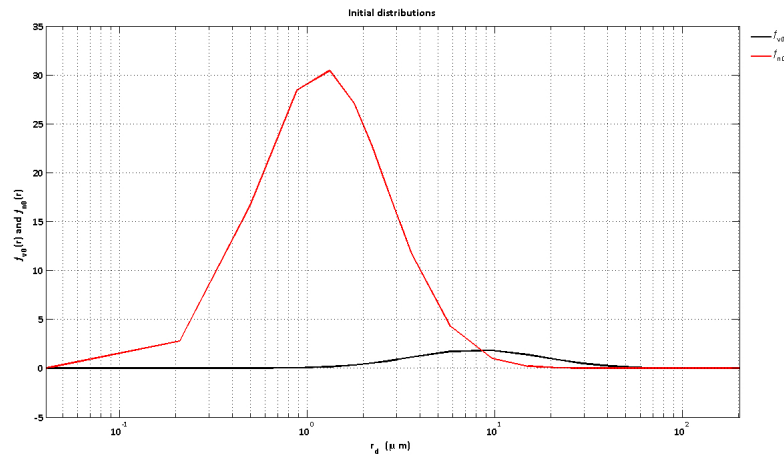


**Figure 10:** Initial Distribution 50-50

Figure 11, shows the separation profile for the height of the column as a function of time at different local volume fractions. From this it can be seen that the local volume fraction from the beginning is near  $\approx 0.50$ . At  $t=20\text{min}$  the local volume fraction is down to 0.30, at  $t=25\text{min}$  the local volume fraction is down to only 0.10, this indicates that this is a rather fast separation.

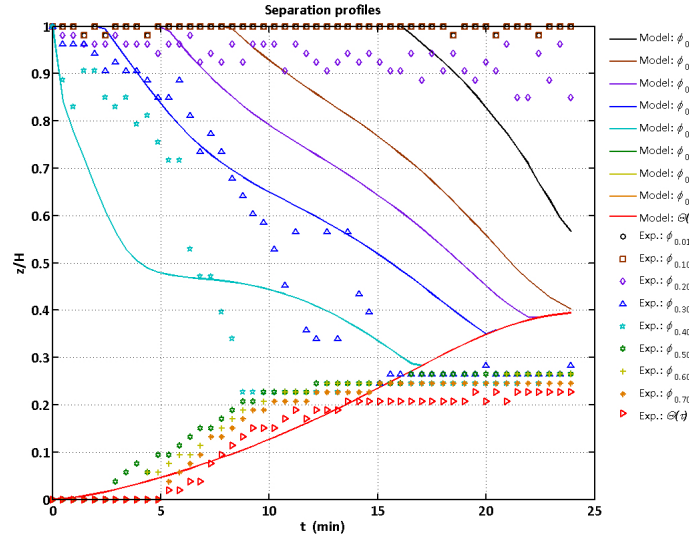


Figure 11: Separation Profile 50-50

In Figure 12, the initial drop growth rate is high throughout the height of the column, then the drop growth rate rapidly plummets. The average number density also confirms that there is an rapid coalescence of droplets initially. The mean droplet radius and the standard deviation indicates that the droplets steadily grow as time increases but then seem to level off as the separation completes. Also, the interface coalescence is happening fast but the binary coalescence between the drops is slow in comparison.

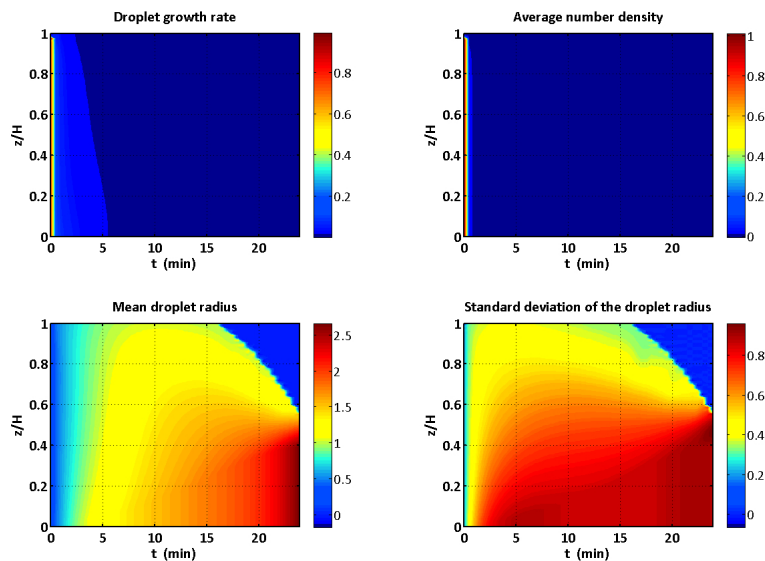


Figure 12: General Contours 50-50

In Figure 13, the velocity of the continuous phase is faster at the later times, and always faster near the interface. As the emulsion separation progresses the droplets grow which increase the volume displacement of the continuous phase. There is a pronounced decrease in the slope at  $z/H=0.4$  as this is the separation interface it eventually goes towards.

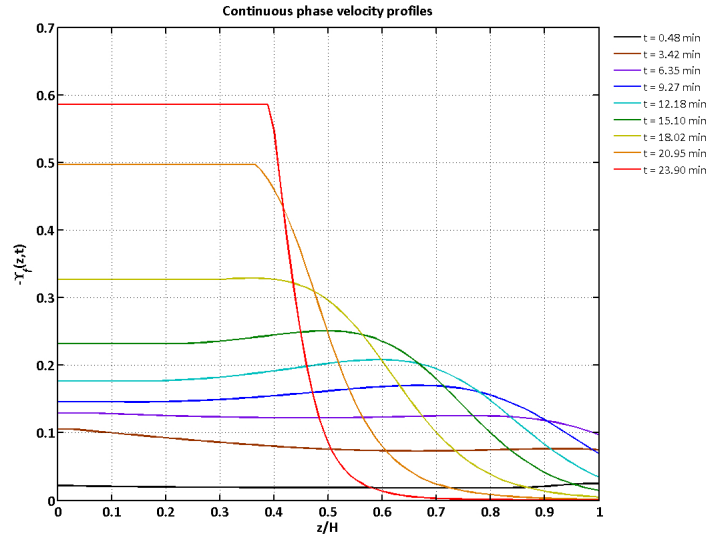


Figure 13: Continuous phase velocity profile 50-50

## 5.4 75/25

The optimized fitted parameters are presented in Table 7. This is for an emulsion with added a blend of 25% Demulsifier 1 and 75% Demulsifier 2 demulsifiers.

**Table 7:** Fitting parameters for 75-25, Demulsifier 1 and Demulsifier 2

Fitting Parameters	
Collision rate constant, $k_{CR}$	0.05
Binary coalescence efficiency constant, $k_{CE}$	0.005
Interfacial coalescence constant, $k_{IC}$	1
Effective diffusion due to compressive stress, $D_{CS}$	5.00E+07

In Figure 14, This is a representation of the initial droplet size distribution. These values were collected from experimental results. The distribution ranges from  $0.1 - 10\mu m$  same as the other examples, this has a slightly higher peak than the 50-50 case.

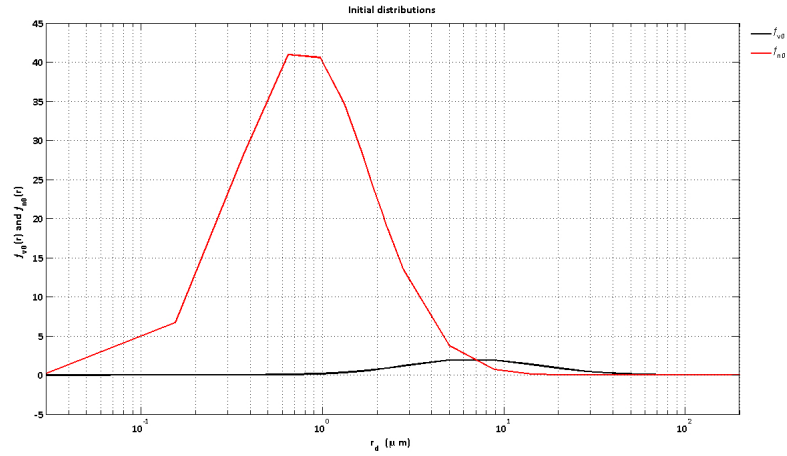


**Figure 14:** Initial Distribution 75-25

In Figure 15, This separation profile shows an notably slow separation. The 0.40 volume fraction slope from the model is not representing the experimental values adequate in this case, as the experimental values are quite scattered. The trend for the separation is much slower than what the 0.40 fraction illustrates. Thus illustrate a rather slow separation.

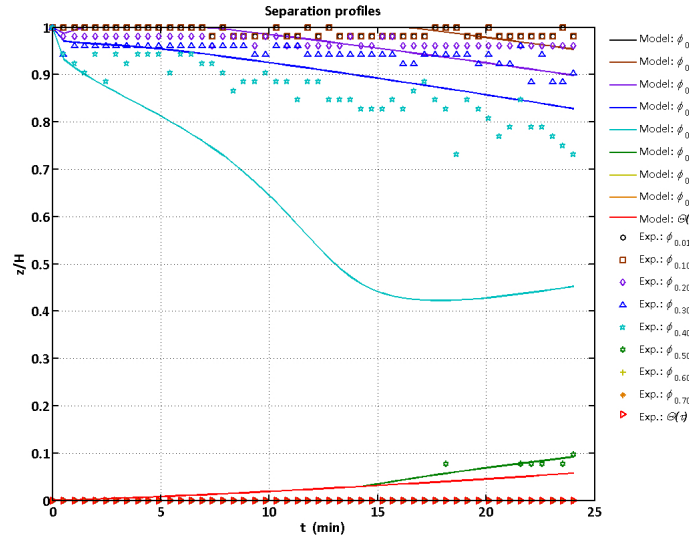


Figure 15: Separation Profile 75-25

In Figure 16, As with the other simulations the drop growth rate and the number distribution decrease rapidly. The standard deviation in this case illustrate that there is only a collection of different size droplets at the very bottom of the emulsion ( $Z \approx 0$ ). It is difficult to determine if there is even a resolved water phase present.

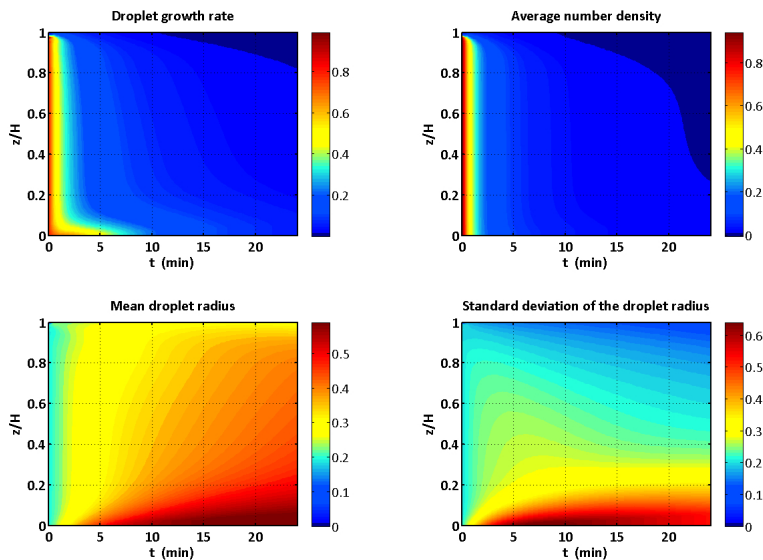


Figure 16: General Contours 75-25

In Figure 17, this continuous velocity phase profile indicates a slow separation profile, with its minute values, however similar trends for this case as the other cases.

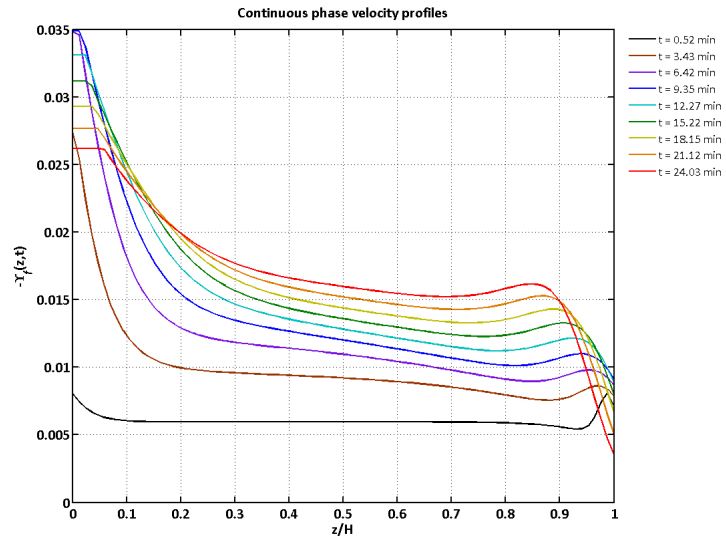


Figure 17: Continuous phase velocity profile 75-25



## 5.5 100-0

This simulation produced unwanted results, the separation profile, general contours and the continuous phase velocity are useless as the something went, with more time and perhaps new experimental results for this case the results would have been usable.

One case of tested fitted parameters are presented in Table 8. This is for an experiment with only Demulsifier 1 as the demulsifier.

**Table 8:** Fitting parameters for 100-0, Pure Demulsifier 1

Fitting Parameters	
Collision rate constant, $k_{CR}$	1
Binary coalescence efficiency constant, $k_{CE}$	0.05
Interfacial coalescence constant, $k_{IC}$	15
Effective diffusion due to compressive stress, $D_{CS}$	1.00E+09

In Figure 18, the initial droplet size distribution is represented for this case with pure demulsifier. This case of experimental values did not simulate well, this resulted in poor results which can not be used in the comparison.

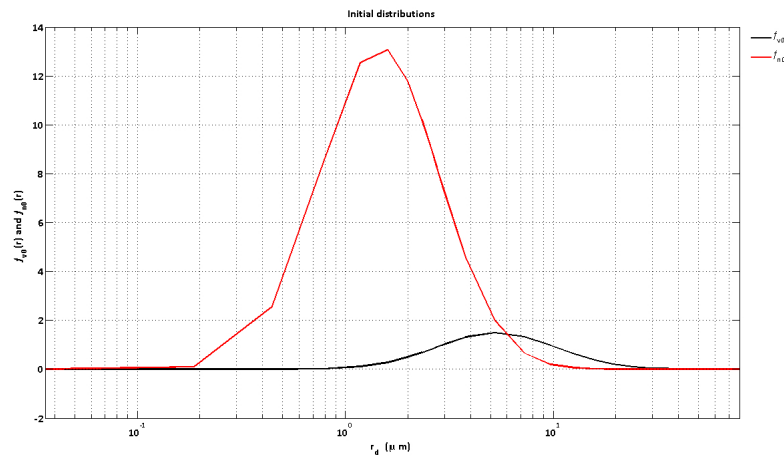


**Figure 18:** Initial Distribution 100-0

In Figure 19, the separation profile for experimental values indicate that the separation as high as a volume fraction of 0.30 is rather quick but any separation fraction lower than that is slow.

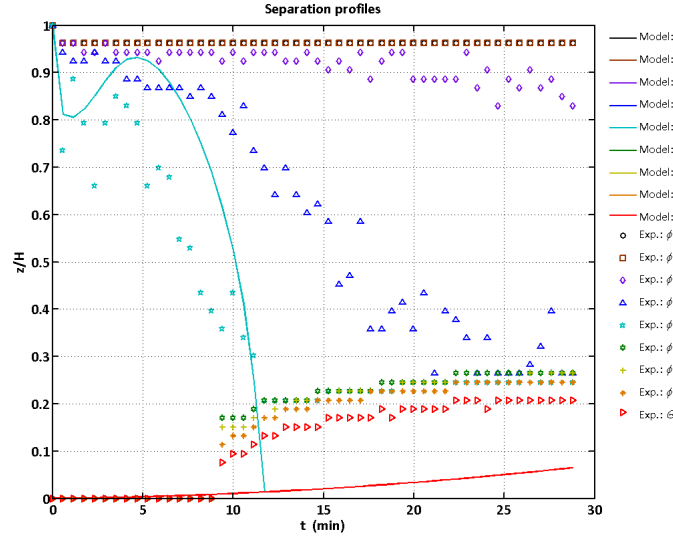


Figure 19: Separation Profile 100-0

In Figure 20 and Figure 21, the figures shows that there is a uniformity throughout the entire height of the column with no separation, which is not the actual results.

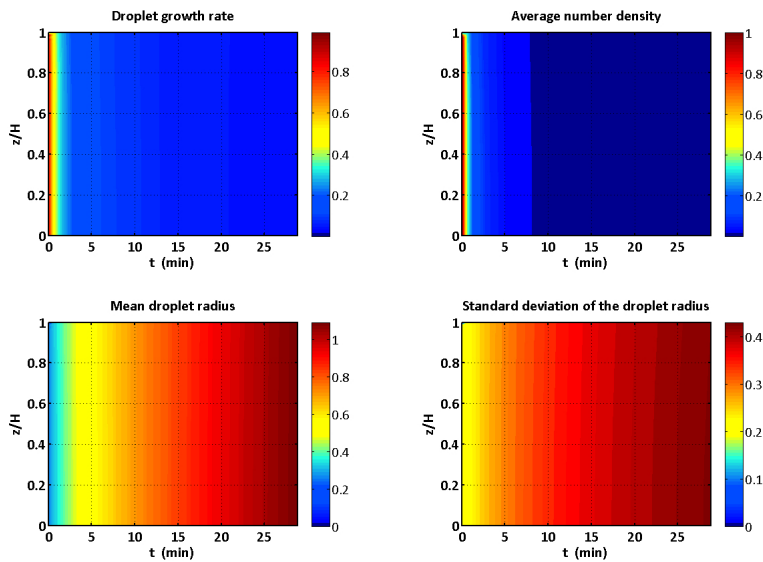


Figure 20: General Contours 100-0

In Figure 21, this continuous velocity phase profile indicates no of velocity with regard to height separator which is not an viable result.

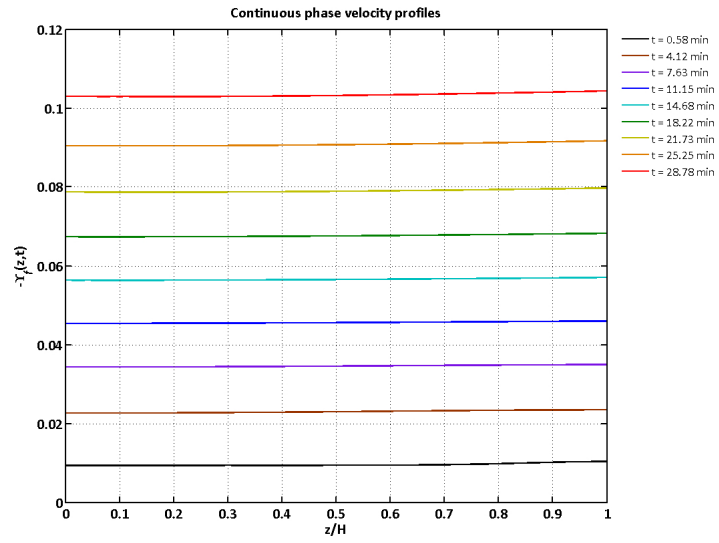


Figure 21: Continuous phase velocity profile 100-0

## 5.6 Comparison

To compare the demulsifier ratios against each other and determine which provide the fastest separation, the maximum values of the continuous phase velocity and drop growth rate was utilized. The maximum value of continuous phase velocity gives a good representation of the fastest sedimentation. The equation for the continuous phase velocity is given in Equation (73), this velocity represents the velocity of the displacement of the sedimentation "layer", not just for single droplet, as it integrates over the product of sedimentation velocity, Equation (14), and the average number density, Equation (44), with regards to the radii, divided by the local continuous phase.

$$U_{f,z} = \frac{1}{1-\phi} \int_0^{r_{max}} U_z(r,z) v f dr \quad (73)$$

Equation (74) is for the drop growth rate. This give a dimensionless indication of the coalescing properties of the separation. The maximum value provide a qualitative parameter for understanding the coalescing attributes regarding separating the emulsion.

$$R_{g,z} = \int_0^{r_{max}} r v R_B dr \quad (74)$$

The comparison of the max sedimentation rate ( $U_{f,max}$ ) and maximum droplet growth rate ( $R_{g,max}$ ) with each case gives a good indication on how the the complete performance of the separation of the emulsion is, however these are dimensionless numbers so these only give good indications and not accurate values. Table 9 displays the maximum values of  $U_{f,max}$  and  $R_{g,max}$  for the different blend ratios and pure demulsifiers, namely Demulsifier 1 and Demulsifier 2.

**Table 9:** Comparison of the  $U_{f,max}$  and  $R_{g,max}$  for each of the cases

Parameter	Demulsifier 1 - Demulsifier 2				
	0-100	25-75	50-50	75-25	100-0
$U_{f,max}$	0.0510	0.0783	0.5971	0.0353	0.1044
$R_{g,max}$	2.7778	13.5944	145.3130	8.4704	54.0598

In Table 10, the table shows an comparison of the initial mean radius ( $\bar{R}$ ) with its standard deviation ( $\sigma_R$ ) for each case. For the blends in the Demulsifier 1 and Demulsifier 2 blend the droplet size is fairly similar, except for 0-100 were the initial droplets are much larger.

**Table 10:** Comparison of the initial mean radii and standard deviation for each of the cases

Parameter	Demulsifier 1 - Demulsifier 2				
	0-100	25-75	50-50	75-25	100-0
$\bar{R}$ [ $\mu m$ ]	51.2429	23.1650	20.8148	19.5845	10.0997
$\sigma_R$ [ $\mu m$ ]	37.6185	23.5111	19.4810	19.8590	7.3950

For the 75-25 case the separation profile (Figure 15) indicated a very slow separation this result coincides with the values for maximum continuous phase velocity, drop growth rate and the smallest initial droplets. From the maximum continuous phase velocity and the maximum droplet growth rate the fastest separation should occur for the 50-50 case, however as shown in the separation profiles, Figure 3 and 11 this is not the case. For the 0-100 case the time for a complete separation is 16min and for 50-50 case the time is over 25min, so the vast difference in separation time comes down to the initial droplet size. The 0-100 case has over twice the initial mean droplet size in comparison with the 50-50 case,  $51.2\mu m$  versus  $20.8\mu m$ , respectively. So this shows that even though the 50-50 case grows faster and sediments at a higher rate, the 100-0 sediments faster because of the initial bigger droplets.



## 6 Conclusion

The population balance predicts the dynamic and spatial evolution of the droplet size distribution across the entire batch separator. The model was used to fit data for local fractions from experimental data in order to compare the model results with actual experimental results.

The prediction of the dynamic and spatial evolution of the drop size distribution allows one to calculate the backflow of the continuous phase and drop growth rate (the first moment of the volume weighted coalescence birth function). These two calculated values allow one to make a semi-quantitative description of the individual sedimentation and binary coalescence rates, based on the types and concentration/composition of demulsifiers or mixtures of demulsifiers used for separation.

The experiment consisted of an water in crude oil emulsion with added demulsifier. Five experiments were tested, with varying ratios of the two different demulsifiers, Demulsifier 1 and Demulsifier 2.

The results for the different demulsifiers demonstrated that pure Demulsifier 2 provided the fastest separation of this water in oil emulsion, this was due to the large initial droplet size in this mix. However, the blend with 50% Demulsifier 1 and 50% Demulsifier 2 had the largest maximum continuous phase velocity ( $U_{f,max}$ ) and maximum drop growth rate ( $R_{g,max}$ ), which resulted in a fast separation, 25min for complete separation as opposed to 16min for the pure chemical Demulsifier 2. The large value of  $U_{f,max}$  indicate fast sedimentation and  $R_{g,max}$  indicate fast binary coalescence, however the large initial droplet size for the pure Demulsifier 2 provided the fastest separation.

This separation model could then be used to develop chemical destabilization strategies to knock out a significant fraction of the emulsified water and reduce process volumes and energy consumption, which could reduce greenhouse gas emissions and improve process economy. Further work could be to include other technological enhancements of the sedimentation processes in the model, such as thermal, centrifugal, chemical, electrostatic, acoustic or electromagnetic separation methods.





## 7 Bibliography

- [1] Thu Phuong Bui. *Master Thesis: Study of the efficiency of commercial and green/yellow demulsifiers on water removal efficiency*. NTNU, 2014.
- [2] C. A. Coualoglou and L. L. Tavlarides. Description of interaction processes in agitated liquid-liquid dispersions. *Chem. Eng. Sci.*, 32(11):1289–97, 1977.
- [3] Tom Frising, Christine Noik, and Christine Dalmazzone. The liquid/liquid sedimentation process: from droplet coalescence to technologically enhanced water/oil emulsion gravity separators: a review. *J. Dispersion Sci. Technol.*, 27(7):1035–1057, 2006.
- [4] B. A. Grimes. Population balance model for batch gravity separation of crude oil and water emulsions. part i: Model formulation. *J. Dispersion Sci. Technol.*, 33(4):578–590, 2012.
- [5] B. A. Grimes, C. A. Dorao, S. Simon, E. L. Nordgard, and J. Sjoblom. Analysis of dynamic surfactant mass transfer and its relationship to the transient stabilization of coalescing liquid-liquid dispersions. *J Colloid Interface Sci*, 348(2):479–90, 2010.
- [6] S. Hartland and S. A. K. Jeelani. Choice of model for predicting the dispersion height in liquid/liquid gravity settlers from batch settling data. *Chem. Eng. Sci.*, 42(8):1927–38, 1987.
- [7] S. Hartland and S. A. K. Jeelani. Prediction of sedimentation and coalescence profiles in a decaying batch dispersion. *Chem. Eng. Sci.*, 43(9):2421–9, 1988.
- [8] Martin Henschke, Lars Holger Schlieper, and Andreas Pfennig. Determination of a coalescence parameter from batch-settling experiments. *Chem. Eng. J. (Amsterdam, Neth.)*, 85(2-3):369–378, 2002.
- [9] Hugo A. Jakobsen, Haavard Lindborg, and Carlos A. Dorao. Modeling of bubble column reactors: Progress and limitations. *Ind. Eng. Chem. Res.*, 44(14):5107–5151, 2005.
- [10] S. A. K. Jeelani and S. Hartland. Effect of dispersion properties on the separation of batch liquid-liquid dispersions. *Ind. Eng. Chem. Res.*, 37(2):547–554, 1998.
- [11] S.A.K. Jeelani and S. Hartland. *The Continuous Separation of Liquid/Liquid Dispersion*. Pergamon Press Ltd, 1993.
- [12] Preben C. Mørk. *Overflate og kolloidkjemi grunnleggende prinsipper og teorier*. NTNU department of chemical engineering Trondheim, 2004.
- [13] J.F. Richardson and W.N. Zaki. *Trans*, volume 32. 1954.
- [14] S. Simons, M. M. R. Williams, and J. S. Cassell. A kernel for combined brownian and gravitational coagulation. *Journal of Aerosol Science*, 17(5):789–793, 1986.
- [15] J.C. Slatter, L. Sagis, and E.-S Oh. *Interfacial Transport Phenomena 2nd ed*. Springer, 2nd ed.
- [16] J. Stoyel and T. Sontvedt. *Stability of emulsions: A model describing coalescence of heavy oils in gravity fields*. Begell House, 1998.
- [17] Hua Wang and Robert H. Davis. Simultaneous sedimentation and coalescence of a dilute dispersion of small drops. *J. Fluid Mech.*, 295:247–61, 1995.